Reconstruction 4D du ventricule à partir de deux cycles cardiaques

4D Reconstruction of the Left Ventricle Using Two Successive Cardiac Cycles

[*]Cl. Bonciu, [*]C. Léger, [*]G. Lamarque, [**]L. D. Nguyen

[*]LESI (Laboratoire d'Electronique Signaux Images)
and GDR PRC–ISIS du CNRS
Université d'Orléans, 12, rue de Blois,
BP 6744, 45067 Orléans Cedex 2, France
E–mail: [bonciu][leger][lamarque]@lesi.univ–orleans.fr

[**]CHRO (Centre Hospitalier Régional d'Orléans)
Boulevard de l'Hôpital, 45100 Orléans, France
E–mail: nguyenld@valcofim.fr

Toute correspondance doit être envoyée à l'adresse suivante :

Christophe Léger
Université d'Orléans, ESPEO/LESI, 12 rue de Blois, BP 6744, 45067 Orléans cedex 02

Reconstruction 4D du ventricule à partir de deux cycles cardiaques

[*]Cl. Bonciu, [*]C. Léger, [*]G. Lamarque, [**]L. D. Nguyen

[*]LESI (Laboratoire d'Electronique Signaux Images)
and GDR PRC–ISIS du CNRS
Université d'Orléans, 12, rue de Blois,
BP 6744, 45067 Orléans Cedex 2, France
E–mail: [bonciu][leger][lamarque]@lesi.univ–orleans.fr

[**]CHRO (Centre Hospitalier Régional d'Orléans)
Boulevard de l'Hôpital, 45100 Orléans, France
E–mail: nguyenld@valcofim.fr

9 août 2001

Résumé: Cet article présente une nouvelle approche de reconstruction du mouvement et de la déformation du ventricule gauche du cœur à partir d'images échographiques. Les images sont acquises pendant deux cycles cardiaques successifs, avec une sonde externe trans–thoracique dont le capteur est mis en rotation. Les contours et volumes ventriculaires sont reconstruits en utilisant des modèles déformables fréquentiels. Une étude détaillée de la forme générale des contours ventriculaires est présentée : elle permet de fixer des critères de cohérence à respecter lors d'une procédure de détection de contours supervisée. Des résultats préliminaires obtenus avec l'assistance d'un expert servent de base pour le développement d'un protocole de reconstruction automatique. Enfin, des expérimentations cliniques ont été réalisées sur un sujet sain. Les résultats obtenus concordent avec ceux d'examens classiques et valident les modèles proposés.

Mots clés : Echographie 4D, imagerie cardiaque, sonde tournante, modèles déformables fréquentiels 2D et 3D.

4D Reconstruction of the Left Ventricle Using Two Successive Cardiac Cycles

[*]Cl. Bonciu, [*]C. Léger, [*]G. Lamarque, [**]L. D. Nguyen

[*]LESI (Laboratoire d'Electronique Signaux Images)
and GDR PRC–ISIS du CNRS
Université d'Orléans, 12, rue de Blois,
BP 6744, 45067 Orléans Cedex 2, France
E–mail: [bonciu][leger][lamarque]@lesi.univ–orleans.fr

[**]CHRO (Centre Hospitalier Régional d'Orléans)
Boulevard de l'Hôpital, 45100 Orléans, France
E–mail: nguyenld@valcofim.fr

9 August, 2001

Abstract: A new approach to reconstruct the left–ventricle movement and deformation from echocardiography images is proposed. Ultrasound images are acquired during two successive cardiac cycles, using a high–speed continuously rotating trans–thoracic probe. The ventricular contours and volumes are reconstructed using frequency–based models. A detailed study of ventricular contour shapes is presented, based on several coherence criteria, used as constraints in a supervised contour detection procedure. Preliminary results on the ventricular dynamics, based on the expert–type knowledge, are detailed. These results are the basis for an automatic reconstruction protocol. Clinical experiments on a healthy human subject are reported. The clinical results are promising, validating the proposed models.

Keywords: 4D ultrasound imaging, heart imaging, rotating probe, frequency–based 2D and 3D deformable models.

1. Introduction

Due to its numerous benefits compared to other cardiac imaging techniques, two–dimensional (2D) echocardiography is widely used in cardiology. The echography does not use ionising radiation and has no known bio–effects in the operation frequency range. It is a non–invasive diagnostic technique, except the trans–oesophageal examinations, where the discomfort effects are still marginal [1]. It also provides real–time acquisition, flexibility of observation, fast examination and accurate physiological measurements. On the other hand, ultrasound imaging is known to induce a significant inter–operator variability and to provide poor quality images, with low signal to noise ratio. This is actually true compared to other imaging techniques such as magnetic resonance imaging or nuclear imaging. Nevertheless, the speckle noise – intrinsic to ultrasound images – can be reduced applying complex filtering techniques for the acquired scan–line signals [2], [3] and/or for the resulted images [4], [5]. To enhance image quality during acquisition, an alternate way consists in injecting contrast agents in the ventricular cavity [6].

Most heart diseases can be observed on ultrasound images, obtained with a fixed 2D probe [7]. Unfortunately, these 2D–images do not provide accurate and reliable measures of the heart cavity volumes [8]. This is due to the cardiac dynamics, which are difficult to quantify with a fixed 2D acquisition system. However, three–dimensional (3D) acquisition systems allow a better characterisation of several major heart functions. Prohibitive acquisition time and computational costs have been recently decreased, allowing clinical use of 3D left ventricle (LV) reconstruction. 3D–imaging systems highly improves visualisation, by providing direct cross–sections of anatomical structures [9]. Usual clinical measures such as ejection fraction, global cardiac flow, intra–cardiac volume–pressure ratio and myocardial mass are now directly obtained with high accuracy with 3D reconstruction systems [10], [11], [12], [13].

In this framework, scanning *in vivo* all the LV volume by an ultrasound beam is still a matter of research in ultrasound imaging. The usual 2½D scanning technique consists in acquiring successive images, located in the 3D space, obtained by moving a 2D acquisition probe. Several results have been reported, using various trans–thoracic or trans–oesophageal 2D–probes. The probes can move in parallel planes [14], oscillate

[15] and rotate [16], [17], [18]. Another approach is to follow the operator free movement with a spatial localisation system for the transducer position [19]. 3D systems based on these different techniques are commercially available, although preferred for static anatomic structures: Combison 530 (Medison–Kretztechnik), HDI 3000 (ATL/Acuson), TomTec (TomTec Imagins systems), Vingmed CFM (Diasonics), Sonos 5500 (Hewlett Packard).

In cardiac imaging, successive images are acquired during multiple heartbeats. Assuming the latter are identical, the images are grouped according to their relative instant during the cardiac cycle. After manual [20] or automatic [18] segmentation of the cavity boundaries, the contours of the endocardium wall are mapped onto a 3D of co–ordinate system. Finally, a modelling algorithm, which uses the detected contours, reconstructs the volume [12], [13], [16], [21], [22].

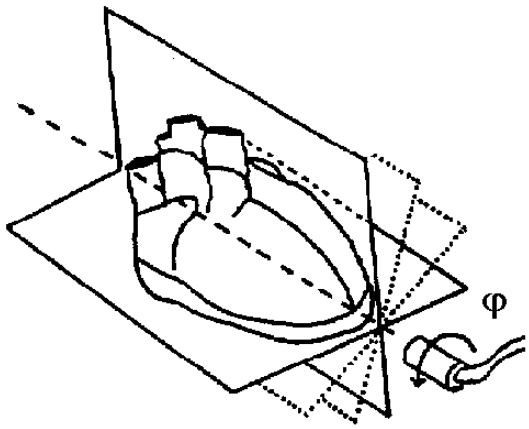

Figure 1: Rotating ultrasound probe (φ is the rotation angle).

In this paper, the proposed device is a trans–thoracic rotating probe (see Figure 1), which acquires cardiac images during two cardiac cycles. This choice offers several main benefits. It is simple to use for the physician, without traumatising the patient, and the probe mechanism does not require expensive nor critical miniaturisation technology. The use of only two successive cardiac cycles increases significantly the validity of the cardiac cycle periodicity hypothesis. Finally, the spatial and temporal periodic movement law of the probe allows natural application of harmonic models to reconstruct the LV boundaries [23], [24], and volumes [25].

Several experiments that use the external rotating 2D probe, specially designed for fast 3D acquisition, are presented in this paper. The description of the probe is the subject of the next section. In section 3, the method used to model the LV contours is detailed. The technique to model the successive LV volumes is explained in section 4. Finally, the last section presents preliminary clinical results, obtained on a healthy human subject.

2. Experimental Device

The 2D spinning probe (Figure 2) has a cylindrical shape, centred on its rotation axis. It is composed of two principal parts: the motor and the ultrasound sensor. The probe is coupled to a standard ultrasound system and with a computer, which performs all the data processing operations.

The electrical motor makes the ultrasound sensor rotate. An optical encoder is used to measure the rotation angle φ of the sensor each 10 ms. The motor rotates continuously at a speed of up to 8.3 rotations per second. The operating speed is set to 4 rotations per second in the experiments detailed in this paper. Due to the twisting of the sensor liaison wires, the motor rotation must be inverted each two rotations. The inversion time is very short (< 2.5 ms) and can be neglected.

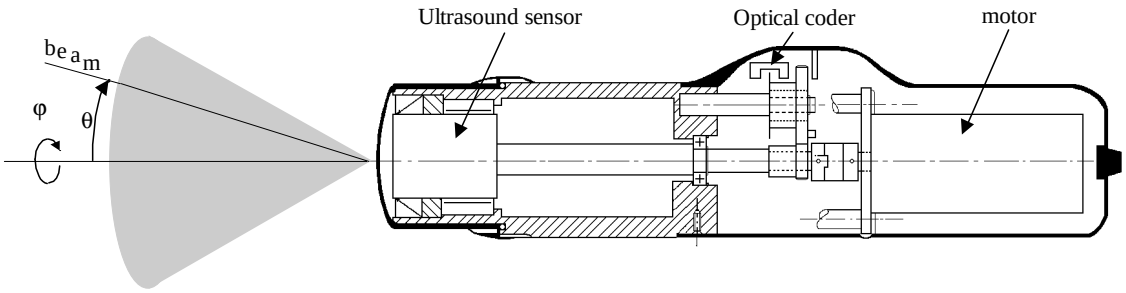

Figure 2: Longitudinal view of the rotating ultrasound probe (φ is the rotation angle and θ is the ultrasound beam angle).

The ultrasound sensor is perpendicular to the rotation axis. It is made up of 64 piezoelectric elements that are lined within a 13 mm segment. Each element is 0.20 mm apart from the others (a half–average ultrasound wavelength). The focal distance is

about 100 mm from the sensor. The frequency bandwidth at 6 dB has the cut–off frequencies at 2.2 MHz and 4.2 MHz. The operating frequency is set to 3.25 MHz, which yields to a penetration depth of approximately 200 mm and to a recovery time of each echo line (at 120 dB) of approximately 0.25 ms.

A suitably delayed impulse electronic excitation of these 64 transmitter–receiver elements generates a deflected ultrasound beam. The angle between the beam direction and the rotation axis is noted θ. The whole angular sector is scanned by one hundred of these consecutive beams, and is about π/3 rad (–π/6≤θ≤+π/6). The acquisition frequency of the system is set to 43 images per second (the frame rate). Consequently, each sector is scanned in 23.3 ms.

While scanning a sector, the sensor rotates. Thus, the images obtained are not perfect plane sections, but conic sections of the LV. The curvature of the surface depends on the ratio r_c between the rotation speed and the scanning speed ($\frac{\Delta \varphi}{\Delta t}$ and $\frac{\Delta \theta}{\Delta t}$, respectively) as shown in Figure 3.

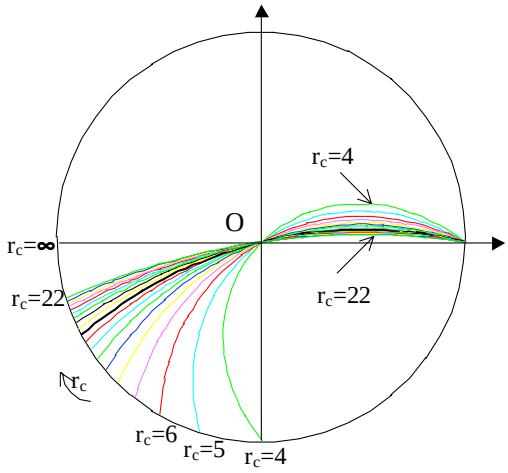

Figure 3: Transversal section of the ultrasound scanning sector, as a function of r_c. r_c is proportional with the ratio $\Delta\theta/\Delta\varphi$. $\Delta\theta/\Delta t$ is the scanning speed and $\Delta\varphi/\Delta t$ is the rotation speed. The thick line represents a typical sector curvature.

The probe is driven by an ultrasound system (ESAOTE AU4) with a specific cardiac module. An internal memory (cineloop) stores up to 100 consecutive digital images, 508 × 508 pixels, 8 bits per pixel depth. Assuming a cardiac frequency of 60

heartbeats per minute, images are acquired during 2 cardiac cycles. Figure 4 presents a typical LV section image and the associated ventricular contour. The technique used to obtain these contours is addressed in the following section.

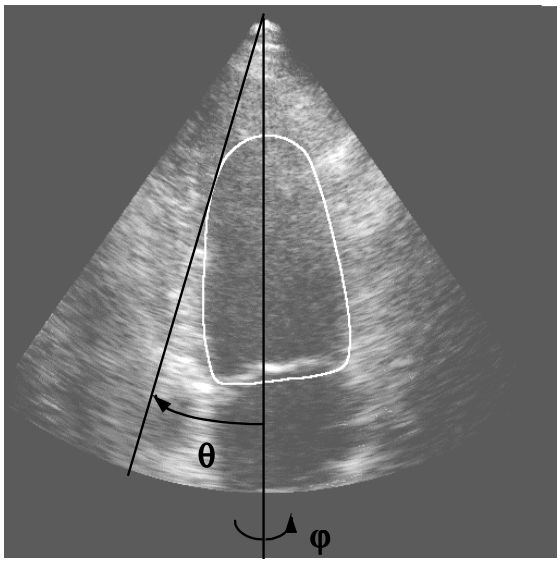

Figure 4: Ultrasound image acquired during the probe rotation (φ is the rotation angle, θ the ultrasound beam angle).

3. Contour Detection Criteria

To improve the quality of the reconstructed LV volume and to facilitate the inclusion of the expert–like knowledge related to the shape of the ventricular contours extracted from each image, consistency criteria have been defined. These criteria refers the spatial and temporal correlation that must exists between the LV contours, and are expressed as weak constraints in the contour detection procedures. These constraints are included in a deformable Fourier–Shannon model, which allows local restricted deformations consistent with an initial frequency model of the polar contour development [24].

In the first stage of this research, hand–drawn contours were modelled in agreement with these criteria and a reference contours database was created. This database allows the qualitative and quantitative study of several deformable contour models. In the present stage, the expert will draw only several systolic and diastolic contours. These contours are subsequently used to define deformation regions in the image sequence.

These regions are used by an automatic contour detection algorithm based on a harmonic active model (HAM) described in [24], [25].

A complete study of the system rotation probe – explored volume [26], [27] has led to the formulation of four consistency constraints. They integrate both the physical aspects of the ultrasound system and the physical knowledge about the LV. These four constraints are: *i*) invariance of the local segmentation criteria, *ii*) contour regularity, *iii*) spatial–temporal deformation regularity, *iv*) spatial–temporal coherence.

3.1. Invariance of the Local Segmentation Criteria

The continuous and fast acquisition means that patterns localised in successive images keep their relative locations in each image. In particular, the local criteria used to trace LV contours must be maintained on successive images. On the other hand, the displacements of some reference pattern in images lead to a displacement of the contour relative to the image.

For example, on the image of Figure 4, the bottom of the mitral valves appears rather bright, as usually on such images. This pattern can be used to fix the bottom of the contour of the LV. If the first traced contour is above the bottom of the mitral valves, the relative correlation between successive images imposes to conserve this criterion for all images in the sequence.

3.2. Contour Regularity

In apical incidence the internal volume of the LV can be compared to a half–ellipsoid. This approximation is usually adopted in echocardiography to model the LV [28]. Contours obtained by cutting a half–ellipsoid by conic surfaces correspond to whole or truncated ellipses. Therefore, without being strictly elliptic, the contour shapes must be regular and smooth.

This constraint is imposed by modelling each contour by a minimal number of parameters [23], [29], [30], [24]. The model is based on the Fourier polar development $\rho(\theta)$ of each contour, around an internal origin from which every radius crosses the contour in only one point. An initial set of contour points, obtained from a hand–drawn contour or an automatic extraction procedure, is processed using a discrete version of the Papoulis smoothing technique [31]. A continuous contour is obtained using cube

spline interpolation. This continuous contour is subsequently modelled using a Fourier–Shannon approach [24], briefly described below.

The model is expressed by the Fourier coefficients or the characteristic samples, obtained using the Shannon optimal interpolation kernel for periodic functions [32]:

$$\rho^N(\theta) = \sum_{n=0}^{N-1} \rho_n \, w^N(\theta, n, N) \tag{1}$$

where

$$w^N(\theta, n, N) = \frac{(-1)^n}{N} \cdot \sin\left(N\frac{\theta}{2}\right) \cdot F_N\left(\frac{\theta}{2} - \pi\frac{n}{N}\right) \tag{2}$$

with

$$F_N(\cdot) = \frac{1}{\tan(\cdot)} \text{ if N is even,} \tag{3}$$

and

$$F_N(\cdot) = \frac{1}{\sin(\cdot)} \text{ if N is odd.} \tag{4}$$

The circular Shannon interpolation function (the interpolation kernel in (3) and (4)) can be also computed using the Discrete Fourier Transform [DFT]. The general (infinite support) Shannon interpolation kernel is defined as the convolution between the discrete contour polar development and the cardinal sine function, i.e. a multiplication with a rectangular window in the frequency domain. An optimally sampled contour with N samples is completely characterised by its M complex Fourier coefficients $\{C_0,\ldots,C_{M-1}\}$, $M=(N+\xi)/2$, where $\xi=1$ if N is odd and $\xi=2$ if N is even. These M coefficients are directly deduced from the M first values $\{S_0,\ldots,S_{M-1}\}$ of the DFT of the sequence $\{\rho_n\}$, $0 \le n < N$, using the relations [23], [29]:

$$C_m = \begin{cases} \dfrac{S_m}{N}, & 0 \le m < M-1 \\ \dfrac{1}{\xi}\dfrac{S_{M-1}}{N}, & m = M-1 \end{cases} \tag{5}$$

where $\xi=1$ if N is odd and $\xi=2$ if N is even.

It can be deduced that the real part of the DFT of the sequence of dimension N, defined by $\{S_0, 2S_1, \ldots, 2S_{M-2}, 2S_{M-1}/\xi, 0, \ldots, 0\}$ is the ideal sampling $\{\rho_n\}$, $0 \le n < N$, of the contour. This sampling can also be obtained by inverse DFT of the whole sequence

$\{S_0,\ldots,S_{N-1}\}$. Moreover, by padding the N values $\{S_0,2S_1,\ldots,2S_{M-2},2S_{M-1}/\xi,0,\ldots,0\}$ with L zero samples, N+L values of the contour $\{\rho(2\pi n/(N+L)\}$, $0\leq n<N+L$ are obtained by inverse DFT [23], [29].

Thus, the initial signal samples can be reconstructed by circular Shannon interpolation by the inverse DFT of the sequence $\{S_0,2S_1,\ldots,2S_{(N/2)-1},2S_{(N+\xi)/2-1}/\xi\}$ padded with as many samples as required. The number of Fourier coefficient parameters directly defines the smoothness of the contour, and their values give its shape.

The origin used for the polar development, named central origin, is chosen to reduce the required number of significant parameters. It is defined as the centre of the largest circle that approximates the contour, in the least square sense, and corresponds to the zero value of the first Fourier coefficient C_1. Its position is near to the centre of inertia of the samples for reasonable smooth contours [23]. In the case of the LV contour shapes (relatively smooth and with good regularity properties), the central origin may be assimilated with the centre of inertia. The iterative algorithm described in [23] produces fast and accurate estimates of the central origin, also due to this geometrical similitude.

A local deformation technique was designed to cope with the active modelling environments. The goal of this technique is to preserve the same frequency model (same number of Fourier coefficients) regardless the position, and within reasonable limits, the strength of the deformation source. Each deformation is performed in an angular sector inside which all the samples are automatically displaced in order to minimise the oscillations of the new contour, relative to the contour outside the deformation sector [24].

In the present case, 32 complex Fourier coefficients provide N=64 characteristic samples, and generate a smooth continuous contour on each image, obtained by circular Shannon interpolation.

3.3. Spatial–Temporal Deformation Regularity

This criterion quantifies the amplitude of the deformations between two successive contours. Given that the LV is continuously deformed with respect to its centre of inertia, which moves continuously during the cardiac cycle, the spatial deformation and the deformation speed are physically restricted to relatively smooth signals.

First, regularity is a function of the acquisition frequency, which must correspond to the LV motion *and* to the acquisition system motion. A quantitative quantification of the relation between the movement parameters of the acquisition system and the allowed dynamics of the deforming object was detailed in [33], based on an analytic signal approach. The derivation of analytic spatial and temporal frequency bounds for the explored object, in the presented acquisition context, is the subject of another distinct report.

Our preliminary results concerning the harmonic complexity of the heart movement showed that the number of 64 characteristic samples gives accurate modelling results [25], [34]. As two successive contours correspond to different acquisition instants, a too low acquisition frequency will increase the amplitude of the acquired deformations, and even may produce sub–sampling artefacts. Moreover, the probe rotation is an additional parameter that can significantly modify the regularity. Indeed, consecutive contours are not acquired at the same angular positions and, consequently, they express different ventricular sections. These 3D effects require a special treatment, mainly due to the increased intra–operator variability encountered in our clinical experiments. When the operator tries to trace the ventricular boundaries for an image sequence, he/she must solve a 3D–projection problem, generated by the probe angular rotation between successive images.

To give an accurate estimate of the LV "normal" deformation in this specific acquisition environment, the amplitude of the LV deformations was estimated using an ellipsoidal LV deformable model. The ellipsoid evolves in a simulated acquisition environment, with parameterised acquisition characteristics (rotation speed, position of the rotation axis, acquisition frequency, etc) [26], [27]. The obtained signals are compared with the real LV deformation signals and estimates of the inter–operator variability may be performed more accurately.

The method used to study the temporal regularity is based on the time evolution of the N characteristic contour samples. Contour models obtained from the image sequence (P images) are developed around their central origin (x_c,y_c) and the $N \times P$ radii $\rho_n(p)$, corresponding to the direction α_n, are analysed. The index n denotes the angular position of the contour in the image, and the index p refers to the contour position in the sequence (Figure 5).

For each angle α_n, the time evolution of the P–1 variations $\rho'_n(p) = \rho_n(p+1) - \rho_n(p)$, is computed. Then the mean μ_n and the standard deviation σ_n of ρ'_n are estimated. The σ_n value is an indicator of the temporal regularity, for the direction α_n. The contour evolution is considered normal when the computed value $|\rho'_n(p) - \mu_n|$ is less than $3\sigma_n$ (7–10 pixels typically). Conversely, a value $|\rho'_n(p) - \mu_n|$ much greater than σ_n (e.g. $4\sigma_n$) indicates a temporal regularity breakdown of the p–th contour in the direction α_n, and is considered as a tracing artefact.

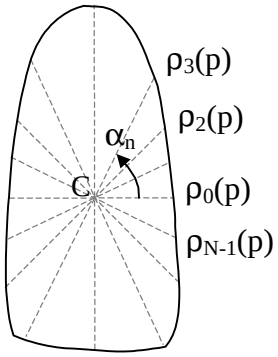

Figure 5: Position of N characteristic samples along the p–th contour, and the corresponding radii $\rho_n(p)$, $0 \le n < N=64$, $0 \le p < P$.

There are two ways to ensure the spatial–temporal deformation regularity. After the first modelling stage, the outlying radii are verified, and the corresponding irregular contours are re–shaped to fit the regularity constraint, expressed in terms of standard deviation. In practice, it is difficult to check the temporal regularity in all the directions α_n at the same time. That is why the horizontal, (α_0, α_{32}), and vertical, (α_{16}, α_{48}), directions are inspected first.

3.4. Spatial–Temporal Coherence

This constraint assumes that the image sequence, particularly the $\rho_n(p)$ signals and, consequently, the deformations of the LV, are periodic. This assumption is based on two hypotheses.

Firstly, the cardiac cycles are supposed to be periodic during the reconstruction active temporal window (less than two seconds). This hypothesis is usual in the clinical investigation case, and is far less restrictive than in the case of the multiple–cycle averaging techniques. Moreover, we use a frequency–based reconstruction technique (a Fourier model) and the potential error introduced by this hypothesis is well distributed along the spatial *and* temporal reconstruction signals. The limited number of Fourier coefficients of the deformable LV model also produces an implicit smoothing of the spatial and temporal signal outliers. This hypothesis is also verified *a posteriori* in the clinical case, using the electrocardiogram (ECG) signal, and, possibly, the two–cycle record is discarded if the patient arrhythmia is too high. The present study uses two cardiac cycles, but preliminary studies on a single cycle fast acquisition are encouraging, opening the possibility of studying clinical cases with more pronounced arrhythmia [35].

Secondly, the probe is assumed to be motionless, in the absolute co–ordinate system. The length of the active acquisition time interval (less than two seconds) and the usual clinical examination context (the patient maintained in apnea) are sufficient conditions for the fulfilment of this hypothesis. This constraint allows the spatial superposition of successive cardiac cycles, and thus, a better wrapping of the exploration space. In the single cycle acquisition method, which is our final goal, the periodicity hypothesis will become less restrictive.

The spatial–temporal coherence can be verified based on these hypotheses. The measures of the rotation angle φ are performed within a normalised temporal cycle ($0 \leq \tau < 1$) on the angular interval ($0 \leq \varphi < \pi$). In this representation, φ is limited to π because only a half–rotation is needed to scan entirely the left ventricle. Mapping all the acquired data on a single normalised cycle, images exhibiting similar spatial and temporal co–ordinates (i.e. similar φ and τ) are better outlined. As a consequence of the periodicity hypothesis, their contours must have similar deformations to be considered as valid data, as it will be illustrated in section 5.

3.5. Supervised Contour Tracing Method

In addition to these previous four modelling constraints, it is necessary that the physician have the possibility to trace the contours according to his/her own expert

criteria. In apical incidence, many contour segments do not appear because they are lost in noise (neat to the apex, for example), are not visible (when the walls do not reflect the parallel echo beams), or do not even exist (when the mitral valves are wide open). Only an expert can therefore trace the relevant contours. Moreover, by allowing the expert to directly supervise the modelling process, i.e. by imposing several desired contours, he/she can provide essential modelling information. For example, he/she can select endocardial or epicardial contours of the LV, including or not the papillary muscles.

As it is unreasonable to require the same results for different experts (inter–operator variability), or the same result for the same expert at different times (intra–operator variability), all the previous hypotheses have been included in a modelling protocol. First, the expert carefully traces the LV contours, for the systolic and the diastolic instants. These contours are modelled using the Fourier–Shannon technique, and then a 4D LV model is constructed [36]. The expert may change this result, if the spatial and/or temporal deformations do not meet the expert criteria. This is performed by the adjustment of one LV contour. The contour may be the original hand–drawn (systolic or diastolic) contour or is obtained by the harmonic active modelling approach [25]. To do that, a sample is moved and this change is extended to the neighbouring samples, spatially as well as temporally. This is done using the Shannon weighting window deduced in [24] for the image cone section and with linear or Gaussian weighting windows for the normal direction to the image and for the temporal dimension. After several trials, the expert becomes familiar with the effect of the spatial–temporal constraints, and fewer corrections are needed.

With the proposed method, the obtained 2D contours are spatially and temporally smoothed, and periodic with respect to the normalised cardiac cycle. Used initially to improve hand–drawn contours, the method is combined with an automatic detection algorithm, and is used concurrently with a spatial–temporal LV model in a complete clinical investigation protocol [25].

4. 4D Reconstruction

The 4D reconstruction of the LV uses the cardiac cycle periodicity hypothesis, as explained in the previous section. Thus, the whole set of data is mapped onto one normalised cardiac cycle.

To reconstruct the LV volume, it is assumed that the latter remains stationary during a very short period of the normalised cardiac cycle. This allows several images, all acquired in the same normalised time interval $\Delta\tau$ in successive cardiac cycles, to be considered spatially coherent. Moreover, if the deformation and movement of the LV is neglected within this time interval, the image set, namely the detected contours can be used to obtain an instantaneous 3D model of the LV. All the contours belonging to the same temporal window $\Delta\tau$ are then used to reconstruct one volume.

We consider for each instant τ_K in the normalised cycle $K=T/\Delta\tau$, temporal windows $\Delta\tau$ centred on τ_K. The LV model can be obtained for all these instants using the contour information from each window. The width of the window gives the number of images used to reconstruct each volume. The wider the window, the greater the number of contours used to reconstruct the volume. Thus, the spatial accuracy increases. However, this implies the use of large temporal windows, and the stationarity hypothesis for the LV becomes unrealistic. Therefore, the window width must be chosen in such a way that the deformations of the LV are small, while providing a maximum number of included contours.

These contours are places in the absolute co–ordinate system, using the probe real rotation law, and the ultrasound beam movement law. They are then placed in a doubly periodic grid whose axes are the beam angular position θ and the probe rotation angle φ, as shown on Figure 6.a. The samples are irregularly spaced in this grid. An interpolation technique, based on the 2D Fourier transform, is applied to complete the grid with the appropriate values [25], [36].

In the present study, the temporal window width $\Delta\tau$ is 5% of the normalised cardiac cycle. This means that we suppose that the LV remains immobile approximately 50 ms. With an acquisition rate of 43 images per second, five (sometimes six) contours extracted from images grouped within two cardiac cycles are used to produce an instantaneous volume. The contours cover well the rotation axis, being approximately

equally spaced. This is true for the acquisition instants that do not suppose a rotation twist of the probe. When this happens, it is possible to obtain two overlapping contours, due to the probe rotation speed changes. This is a drawback of the method, and is produced by physical constraints of the acquisition device, and is still a matter of research. The drawback may be alleviated in two ways. First, another ultrasound probe, using wireless signal transmission, will allow the full continuous rotation of the probe during acquisition. Second, another frequency model, based on a 3D Fourier model (two spatial variables and one temporal variable), preliminarily reported in [25] will eliminate the stationarity hypothesis.

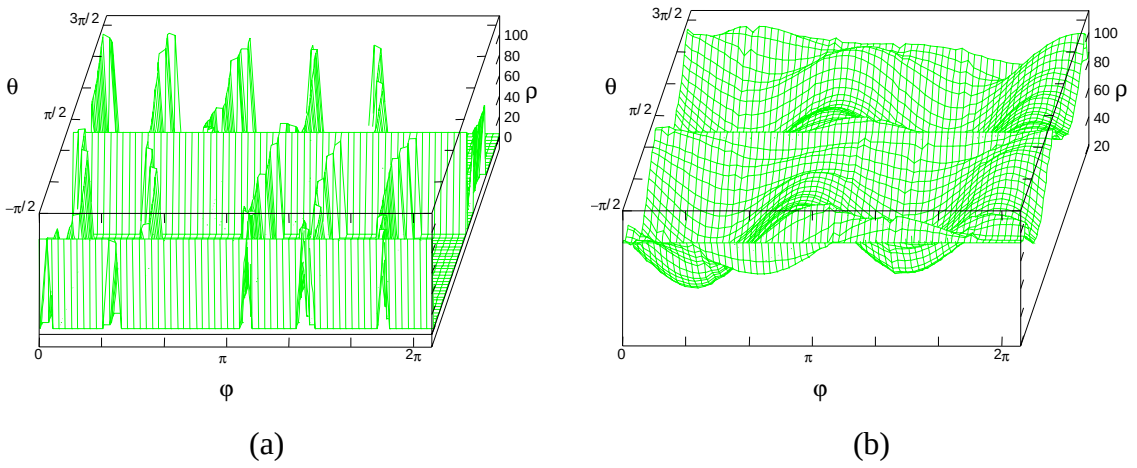

Figure 6: Reconstruction of missing data. (a): initial 3D data, $\{\rho_i, \theta_i, \varphi_i\}$, $0 \le i < n$, with missing data set to zero. (b): surface d(m,n) completed after 97 iterations.

An iterative algorithm progressively forces the 2D harmonic model to fit the original samples of the grid [25][36], and fill the missing data points. This algorithm allows a complete diffusion of initial information d(m,n), over all the data grid, using the Fourier discrete global transformation (Figure 6.b). This modelling technique makes a mild assumption about the LV characteristics: namely that the LV must have a known upper frequency bound in both spatial and temporal harmonic representations. Once the grid is completed, the whole LV may be visualised.

The same technique is applied for successive temporal windows $\Delta\tau$ and the whole LV time evolution is obtained. The global movement is given by the evolution of the centre of inertia of the volumes. The restitution is in good agreement with other reconstruction techniques.

5. *In Vivo* Study

5.1. Experimental Context

The clinical experiment was carried out in the cardiology department of the Regional Hospital of Orléans (France), on a healthy human subject. Recordings were made for two consecutive cardiac cycles. The periods of these cardiac cycles were measured *a posteriori*. The obtained values are equal to 1045±3 ms. In Figure 7, it appears that the overlapped parts of the corresponding ECG signals match, indicating an acceptable deformation periodicity.

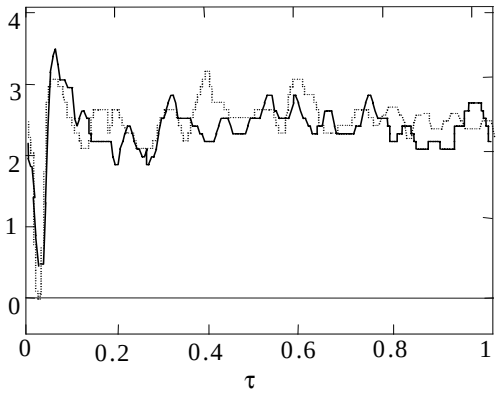

Figure 7: Superposition of two cardiac cycles in normalised time τ ($0 \leq \tau < 1$).

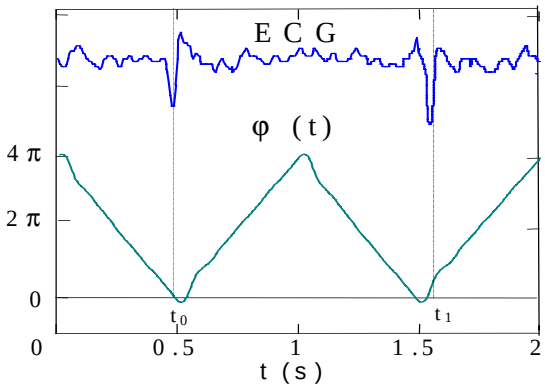

Figure 8: ECG signal and probe rotation angle φ as a function of time.

As shown in Figure 8, the rotation of the probe is not synchronised with the QRS wave of the ECG signal. This is particularly advantageous for patients with significant arrhythmia. Moreover, this increases the angular coverage of the LV, and improves the angular data distribution in the (θ,φ) modelling space. In this purpose, it is also possible to use a QRS–synchronised acquisition system, and to expressly design a constant phase–shifted synchronisation procedure. When the images corresponding to same normalised time in successive cycles have different φ angles, the accuracy of the modelling technique increases and also the computational complexity is reduced (the number of iterations of the reconstruction algorithm is minimal for uniform data distributions). On the ECG record, the two vertical lines indicate the instants t_0 and t_1 of the QRS wave rising front. t_0 is the origin of the normalised time (Figure 8). The

ultrasound probe rotates four times per second (8π rad/sec) and the rotation is inverted every half–second.

In Figure 9, the set of scanned sections is plotted over the normalised cardiac cycle. Each segment outlines the active ventricular sector $\Delta\varphi_n$, i.e. the sector corresponding to the interior of the left ventricular cavity, during the acquisition of the *n*–th image. The middle of the segment indicates the normalised instant τ_n when the ultrasound beam coincides with the rotation axis of the probe (θ=0).

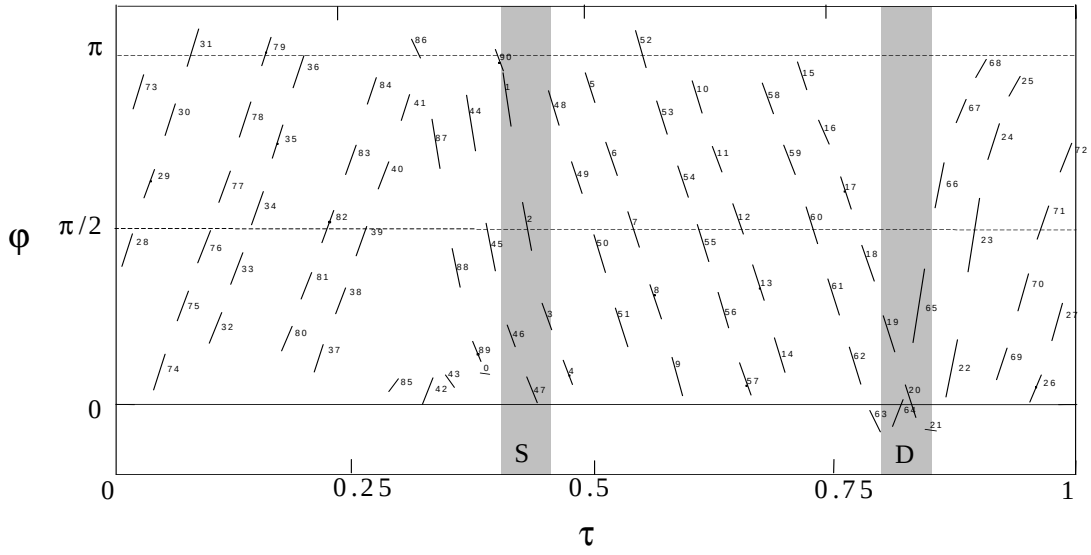

Figure 9: Active scanned segments representation in the (φ,τ) plane for the superposed cardiac cycles. The probe rotation angle φ varies between $0 \leq \varphi < \pi$ (half–rotation). The normalised time τ varies between 0 and 1. Greyed windows D and S represent the end–diastole and end–systole heart phases. The integer index of the image (in the natural acquisition order) is written near to each segment.

The quality of all the recorded images allows the detection of the ventricular wall on each image using the expert knowledge and specific active modelling techniques [25]. All contours are totally included in the apical windows scanned by the ultrasound beam. This context is obtained by the careful alignment of the axis of the probe with the mean LV axis during the active acquisition time interval.

Once the contour detection process is performed, all the contours that belong to the same window of analysis are grouped. Figure 10 presents the end–diastolic images and contours obtained in the end–diastolic phases for the analysed cardiac cycles (D in Figure 9). Similarly, Figure 11 shows the end–systolic images.

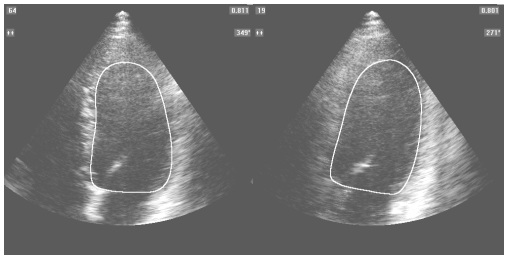

Figure 10: Modelled contours corresponding to the diastole for two successive cardiac cycles.

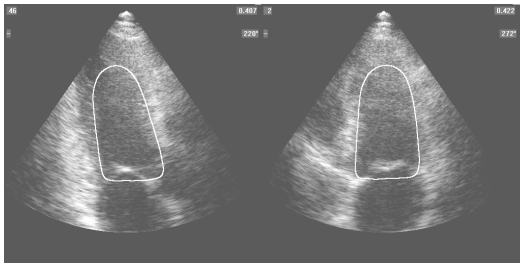

Figure 11: Modelled contours corresponding to the end–systole for two successive cardiac cycles.

5.2. Experimental Results

We use here reference hand–drawn contours, subsequently modelled using the Fourier–Shannon technique described in section 3.2. The temporal evolution of contour radii for several selected directions gives important information about the expected LV model dynamics, obtained with the automatic modelling technique. The 1D analysis is used to validate the parameters of the 2D and 3D deformation models. For example, Figure 12 shows the time variations of the horizontal radii, $\rho_0(p)$, $\rho_{32}(p)$, as well as the abscissa of the central origin $x_c(p)$ of the contour sequence, in an absolute system of co–ordinates.

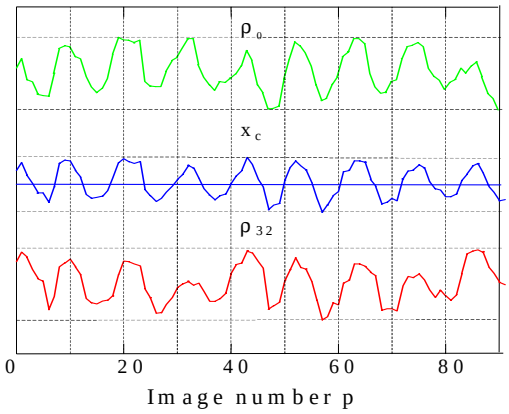

Figure 12: Time variation of the horizontal radii $\rho_0(p)$ and $\rho_{32}(p)$, and the abscissa $x_c(p)$ of the central origin.

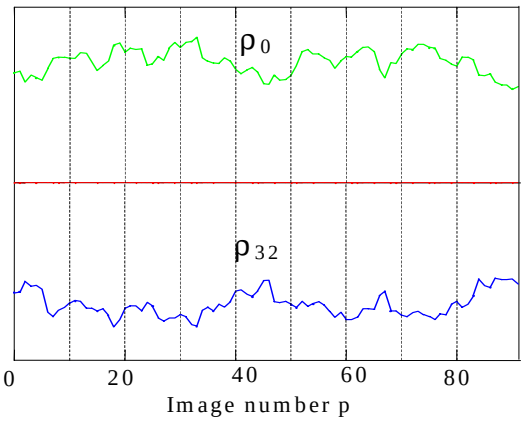

Figure 13: Time variation of the horizontal radii $\rho_0(p)$ and $\rho_{32}(p)$, relatively to the abscissa $x_c(p)$ of the central origin.

The radii variations are sensitive to the probe rotation movement. Namely, a sinusoidal variation appears when the axis of the probe is parallel but not strictly aligned with the LV axis. The sine–like signal period is equal to the period of the probe rotation. The amplitude gives a measure of the ventricular axis displacement. To

attenuate these added sinusoids, the radii $\rho_0(p)$ and $\rho_{32}(p)$ can be represented relatively to the abscissa of the central origin $x_c(p)$, which roughly correspond to a LV local co–ordinate system (Figure 13). In this way, the LV transverse diameter $|\rho_0(p) - \rho_{32}(p)|$ may be approximated at each acquisition instant, and the regular beat of the LV can be observed. These different views give information about the global movement of the LV (provided by the central origin movement in an absolute co–ordinate system) and on the local deformation model (given by the radii variation with respect to the central origin). This global–local decomposition is of main interest in the heart diseases diagnose [7].

Similarly, Figure 14 shows the time variations of the vertical radii, $\rho_{16}(p)$, $\rho_{48}(p)$, as well as the ordinate of the central origin $y_c(p)$. These ordinates are quite insensitive to the rotation of the probe, because the probe and LV axes almost coincide (the maximum angle between axes is less than 10°) during the acquisition. The LV deformations are more evident in the mitral valves neighbourhood ($\rho_{48}(p)$ in figure Figure 14), and almost zero near the apex ($\rho_{16}(p)$). Nevertheless, the LV vertical global oscillation during the cardiac cycles can be observed.

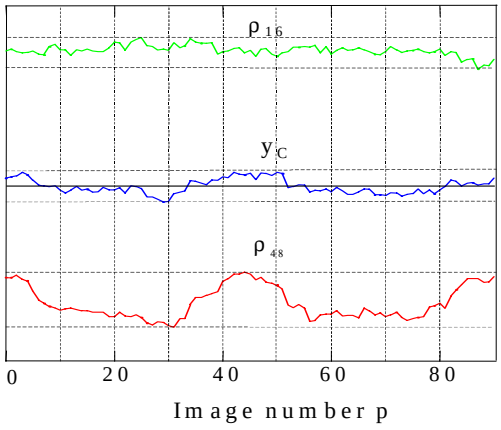

Figure 14: Time variation of the horizontal radii $\rho_{16}(p)$ and $\rho_{48}(p)$, and the ordinate $y_c(p)$ of the central origin.

Using the reference contours obtained for the two–cycle image sequence, the reconstruction of the volume is performed for each instant τ_k. All the obtained static volumes (Figure 15) are animated and the LV motion and deformation can be visualised, using coloured differential maps. A red–green deformation scale is used to provide a direct interpretation of the deformation during animation.

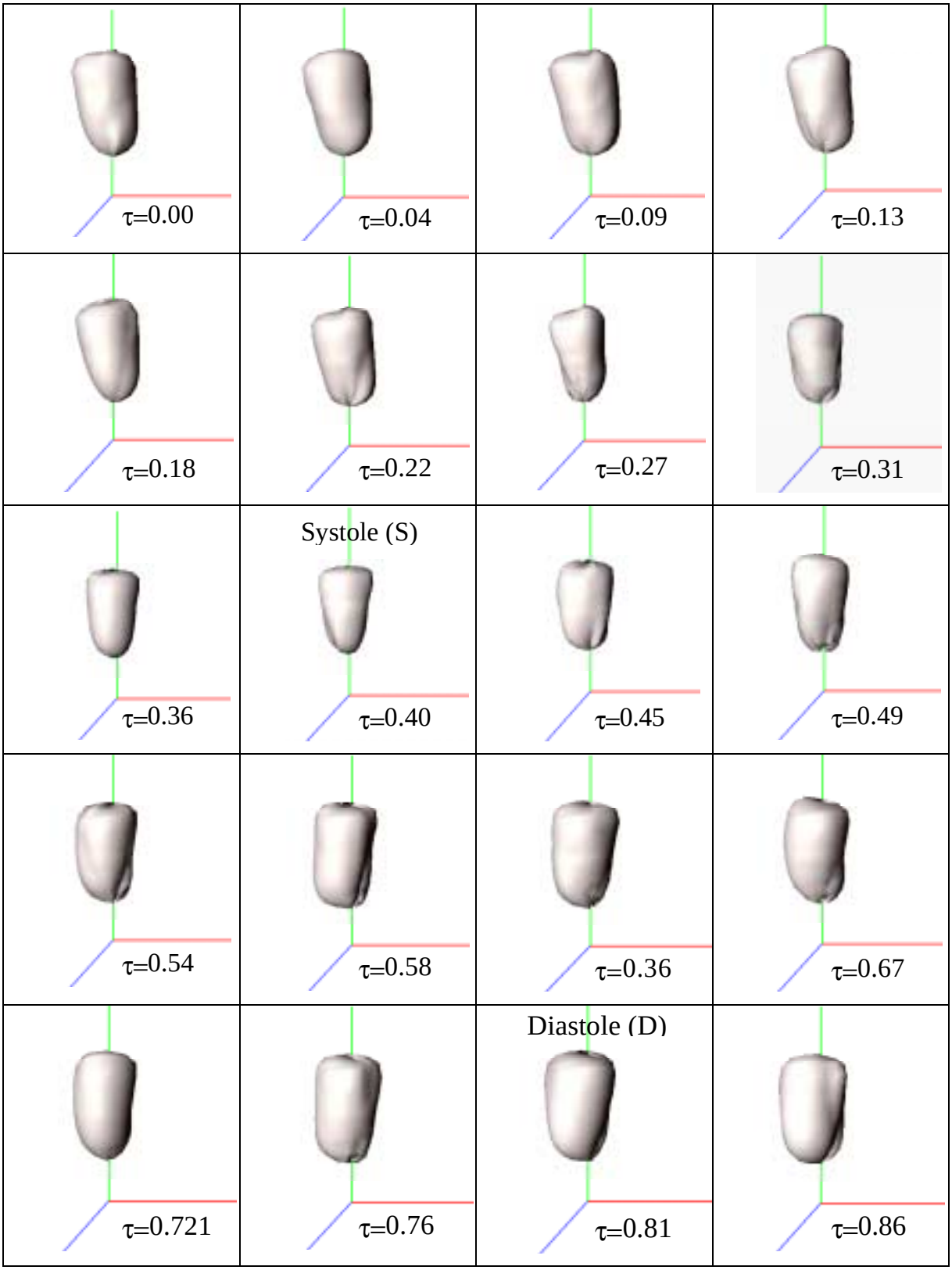

Figure 15: Example of the LV model time evolution. τ is the normalised time ($0 \leq \tau < 1$) corresponding to a cardiac cycle (without differential colour maps).

The red colours give positive deformations and the green ones the negative deformation relative to the previous volume in the sequence. It is noteworthy to outline here that the reconstruction is performed at each instant τ_k. The obtained LV models differs only due to a single different contour that is included in each 3D reconstruction procedure. Consequently, with this sliding window technique, only this new information is distributed spatially and produces an accurate differential colour map.

5.3. Clinical Measures

One of the most used clinical parameter is the ejection fraction, obtained from the end–diastolic and end–systolic volume measurements. The end–diastolic volume V_D is an important measure, which indicates a volumetric overload or abnormal myocardial contractility. The end–systolic volume V_S is a derived measure, which depends on the end–diastolic volume, on the myocardial contractility and on the volume overload. The systolic ejection volume V_{se} and the ejection fraction F_{ej} is estimated form the direct measurements of V_D and V_S volumes (Figure 16) following the equations:

$$V_{se} = V_d - V_s \tag{6}$$

$$F_{ej} = \frac{V_{se}}{V_d}. \tag{7}$$

Each volume is obtained from the corresponding modelling surfaces d(m,n) (as in Figure 6.b) using appropriate scale factors for the image pixel grid, provided by the echocardiography system. A simple numerical integration method is used to obtain the corresponding integral once all the missing data points are estimated by the LV model data values [36].

End–diastolic and end–systolic volumes are respectively V_D=103.5cm^3 and V_S=37.5cm^3, and F_{ej} equals 0.637. Another independent measure of the ejection fraction was available (F_{ej} = 0.617), which is in good agreement with the measure obtained from the 3D reconstruction.

The reconstruction results are obtained using a personal computer, with an Intel Pentium Pro processor working at 200Mhz inside. The processing time of the all volume sequence is about 2 minutes, given the detected contours. In the interactive correction stage, a single modelled volume is obtained in approximately 1.5 seconds.

This is an acceptable time for the interactive reconstruction software. Better results may be obtained with a more advanced hardware support.

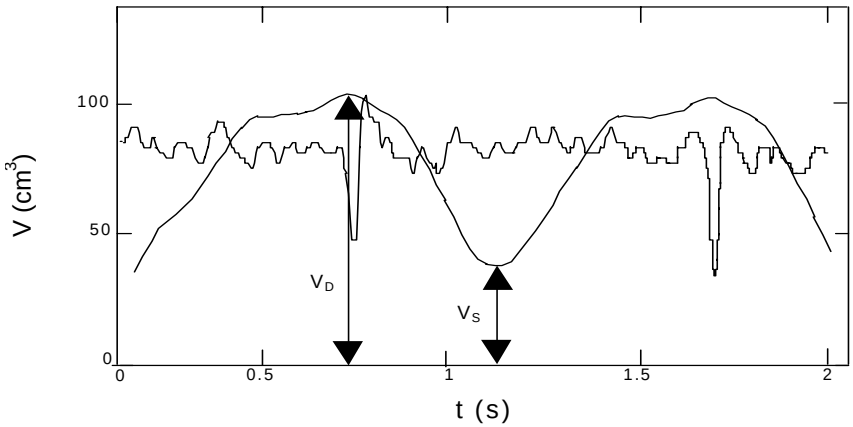

Figure 16: Time evolution of the LV volume in normalized time τ, ($0 \leq \tau < 1$). V_D and V_S represent the end–diastolic and end–systolic volumes.

This experiment confirms the efficiency of the proposed reconstruction method. The reference 2D contours were used to estimate the cut–off frequency of the model, and to test its capabilities on real clinical data.

6. Conclusion

This paper presents preliminary results obtained on the LV spatial–temporal reconstruction, using ultrasound images acquired during only two consecutive cardiac cycles. A trans–thoracic probe has been developed for this purpose. The probe rotates continuously and acquires apical images of the LV at different angles.

The probe is designed for high frequency acquisition systems, and does not require a recovery time as in the case of step–by–step movement probes. The acquisition frequency is limited only by the physical propagation time of the ultrasound beam through the tissues, which is a function of the exploration depth. Consequently, the probe may be used to acquire data about deformable objects, with a given upper bound on the spectral distribution of the spatial and temporal data points. This harmonic constraint is, however, a mild constraint, fulfilled in almost all the domains of clinical ultrasound, including the targeted application area, the echocardiography.

A specific harmonic modelling technique was developed to cope with the complexity of the reconstruction problem, which produces non—uniform data distribution in the reconstruction space. In this paper, the technique is briefly discussed and applied to a reference data set.

In order to extract the expert information and to use this type of information in the modelling process, several coherence criteria have been defined. These criteria have been transformed into coherence constraints in the clinical investigation protocol. These constraints are imposed to the experts to minimise inter– and intra–operator variability during the supervised contour detection procedure. These constraints are also used by an automatic detection procedure, which is the subject of another distinct report.

The proposed approach has the advantage of using only two cardiac cycles and avoids thus the averaging effects encountered in other reconstruction techniques. Our future research will focus on a single cycle modelling technique. Preliminary results [35] are encouraging. The rotation speed of the sensor is increased to eight rotations per cardiac cycle. Thus, three LV contours, angularly separated by $\pi/3$ rad are used to obtain an instantaneous LV volume.

Another advantage of the proposed methods is the interactive adjustment of the resulted volume, when the image quality is not sufficient for an accurate contour detection, or when the detection does not match the medical criteria. The study will be carried on a significant set of patients without requiring the periodicity hypothesis, using a single cardiac cycle. This will open the possibility of developing an accurate study of pronounced arrhythmia, so often encountered in the heart diseases.

7. Acknowledgements

The authors wish to thank the ANVAR (Agence Nationale de Valorisation de la Recherche, France) for its involvement and financial support in this research project.

8. References

[1] L. Pourcelot, M. Lethiecq, F. Patat, F. Tranquart, M. Berson, D. Cathignol, J. Y. Chapelon. Medical ultrasound application. *REE*, 8:68-73, 1997.

[2] A. N. Evans and M. S. Nixon. Mode filtering to reduce ultrasound speckle for feature extraction. *IEEE Proceedings: Vision, Image and Signal Processing*, 142(2):87-94, April 1995.

[3] Thomas R. Nelson and Dolores H. Pretorius. 3D ultrasound image quality improvement using spatial compounding and 3D filtering. *Medical Physics*, 21(6):998-999, 1994.

[4] D. C. Crawford, D. S. Bell, and J. C. Bamber. Compensation for the signal processing characteristics of ultrasound B-mode scanners in adaptative speckle reduction. *Ultrasound medical Biology*, 19(6):469-485, 1993.

[5] S. Leeman and D. A. Seggie. Speckle reduction via phase. *Int. Symp. on Pattern Recognition and Acoustical Imaging*, SPIE:768:173-177, 1987.

[6] N. de Jong, Improvments in ultrasound contrast agents, *IEEE Engineering in Medicine and Biology*, November/December 1996, pp. 72-81.

[7] N. Shiller, P. Shah, M. Crawford, A. DeMaria, R. Devereux, H. Feigenbaum, H. Gutgesell, N. Reichek, D. Sahn, IK. Schnittger, N. Silverman, and A. Tajik. Recommendations for quantitation of left-ventricle by two dimensional echocardiography: American society of echocardiography committee in standards subcomitee. *Journal of American Society of Echocardiography*, 2:358-367, 1989.

[8] A. Fenster and D. Downey. 3-D ultrasound imaging: a review. *IEEE Engineering in Medicine and Biology*, 15(6):41-51, 1993.

[9] F. Hottier and A. Collet Billon. 3D echography: status and perspective. *3D Imaging in Medicine: Algorithms, Systems, Applications*, pp. 21-41, 1990.

[10] J. B Seward, M. Belohlavek, P. W. O'leary, D. A. Foley, and J. F. Greenleaf. Congenital heart disease: wide-field, three-dimensional, and four-dimensional ultrasound imaging. *American Journal of Cardiac Imaging*, 9(1):38-43, 1995.

[11] A. Salustri and J. R. Roelandt. Ultrasonic three-dimensional reconstruction of the heart. *Ultrasound in Medicine and Biology*, 21(3):281-293, 1995.

[12] J. F. Greenleaf, M. Belohlavek, T. C. Gerber, D. A. Foley, and J. B. Seward. Multidimensional visualization in echocardiography: an introduction. *Mayo Clinic Proceedings*, 68:213-220, 1993.

[13] M. Belohlavek, D. A. Foley, T. C. Gerber, T. M. Kinter, J. F. Greenleaf, and J. B. Seward. Three- and four- dimensional cardiovascular ultrasound imaging: a new era for echocardiography. *Mayo Clinic Proceedings*, 68:221-240, 1993.

[14] M. Matsumoto, M. Inoue, S. Tamura, K. Tanaka, and H. Abe. Three-dimensional echocardiography for spatial visualization and volume calculation of cardiac structures. *J. Clin. Ultrasound*, 9(4):157-165, April 1981.

[15] R.W. Martin, G. Bashein, P.R. Detmer, and W.E. Moritz. Ventricular volume measurement from a multiplanar transesophageal ultrasonic imaging system: an in vitro study. *IEEE Transactions on Biomedical Engineering*, 37(5):442-449, May 1990.

[16] H.A. McCann, J.C. Sharp, T.M. Kinter, C.N. McEwan, C. Barillot, and J.F. Greenleaf. Multidimensional ultrasonic imaging for cardiology. *Proceedings of the IEEE*, 76(9):1063-1071, September 1988.

[17] Y. F. M. Nosir, P.M. Fioretti, W.B. Vietter, E.Boersma, A.Salustri, J.T. Postma, A.E.M. Reijs, F.J. Ten Cate, and J. R. T. C. Roelandt. Accurate measurement of left ventricular ejection fraction by three-dimensional echocardiography. a comparison with radionuclide angiograph. *Circulation*, 94(3):460-466, August 1996.

[18] G. Coppini, R. Poli, and G. Valli. Recovery of the 3-D shape of the left ventricle from echocardiographic images. *IEEE Transactions on Medical Imaging*, 14(2):301-317, June 1995.

[19] Thomas R. Nelson, Dolores H. Pretorius, M. Sklansky, and S. Hagen-Ansert. Three- dimensional echocardiographic evaluation of fetal heart anatomy and function: acquisition, analysis and display. *JUM*, 15:1-9, 1996.

[20] T. Gustavson, R. Pascher, and K. Caidahl. Model based dynamic 3D reconstruction and display of the left ventricle from 2D cross-sectional echocardiograms. *Computerized Medical Imaging and Graphics*, 17(4/5):273-278, 1993.

[21] W.E. Moritz, A.S. Pearlman, D.H. McCabe, D.K. Medema, M.E. Ainsworth, and M.S. Boles. An ultrasonic technique for imaging the ventricle in three dimensions

and calculating its volume. *IEEE Transactions on Biomedical Engineering*, 30(8):482-491, 1983.

[22] L. D. Cohen and I. Cohen. Finite--element methods for active contour models and balloons for 2D et 3D images. *IEEE Transactions on Pattern Analysis and Machine Intelligence*, 15(11):1137-1147, November 1993.

[23] C. Léger, J. Thiel, R. Lédée, F. Patat, and L. Pourcelot. Fourier modeling of the left ventricle parasternal boundary. *Traitement du Signal*, 11(2):155-169, 1994.

[24] Cl. Bonciu, C. Léger, J. Thiel, A Fourier–Shannon Approach To Closed Contours Modelling, *BioImaging*, IOP Publishing Ltd., 1998, *to appear.*

[25] Cl. Bonciu. 4D reconstruction of the heart left ventricle using echocardiography images, Ph. D. Thesis, Orléans University, France, December 1997.

[26] Cl. Bonciu and Cr. Bonciu. Aspects concernant l'exploration 2D et 3D par ultrasons. *Bulletin de l'Université de Iasi*. 3(3-4), 1997.

[27] Cl. Bonciu, C. Léger, G. Lamarque, R. Weber, 4D Visualization of the Left Ventricle, Using a Rotating Ultrasound Probe During 4 cardiac cycles, *Computer Information Technology*, vol.6, no.6, 1998, *to appear*.

[28] J. Seema, W. Karl, and A. Willsky. Estimation of dynamically evolving ellipsoids with applications to medical imaging. *IEEE Transactions on Medical Imaging*, 14(2):249-258, 1995.

[29] C. Léger, J. Thiel, C. Bonciu, R. Lédée, J. Fantini, G. Lamarque, Caractérisation d'une surface fermé convexe par interpolation de Shannon circulaire, *4ièmes Journées ORASIS*, Mulhouse, 1993.

[30] Cl. Bonciu, J. Thiel, and C. Léger. Modélisation interactive d'un contour fermé déformable. *Colloque AGI'96*, 1996.

[31] A. Papoulis, *Signal analysis*, McGraw-Hill Inc, ISBN 0-07-048460-0, 1977, p. 329-334.

[32] T. Schanze, Sinc interpolation of discrete periodic signals, *IEEE Transactions on Signal Processing*, vol.43, N° 6, 1995, pp. 1502-1503.

[33] Cl. Bonciu, S. Treuillet, W. Ohley, Reconstructing periodic evolving ellipsoid from 2D slices by a signal processing approach, *Congrès RFIA'98*, Clermont-Ferrand, France, Janvier, 1998.

[34] Cl. Bonciu, J. Thiel, Visualisation 4D de ventricule gauche du cœur par sonde échocardiographique tournante pendant 4 cycles cardiaques, *Colloque AGIS'97*, Angers, France, 1997.

[35] Cl. Bonciu, R. Weber, L.D. Nguyen, 4-D Reconstruction of the Left Ventricle From a Single Cycle Ultrasound Acquisition, *EUSPICO 98*, Greece, *to appear*.

[36] Cl. Bonciu, R. Ledee, S. Treuillet, Reconstruction du ventricule gauche en échocardiographie 4D par modèle déformable, *9ème forum Génie Biologique et Médical*, Brest, France, 1998.